Hybrid Solar Cells Using HgTe Nanocrystals and Nanoporous TiO$_2$ Electrodes**

By *Serap Günes,* Helmut Neugebauer, Niyazi Serdar Sariciftci,* Jürgen Roither, Maksym Kovalenko, Georg Pillwein*, and *Wolfgang Heiss*

HgTe nanocrystals are demonstrated to increase the photon-harvesting efficiency of hybrid solar cells over a broad spectral region between 350 and 1500 nm. Devices combining two solar cell concepts, a solid-state nanocrystal-sensitized solar cell and a nanocrystal/polymer-blend solar cell, are described. These devices give incident photon to current efficiencies up to 10 % at around 550 nm monochromatic irradiation and short-circuit current densities of 2 mA cm^{-2} under simulated AM1.5 (100 mW cm^{-2}) illumination (AM: air mass).

1. Introduction

Nanocrystals of inorganic semiconductors are well suited to the development of novel optoelectronic devices because of their simple processability combined with their optical properties. As a result of strong quantum confinement, they exhibit photoluminescence with high quantum efficiencies, and their emission peaks, as well as the onset of absorption, are strongly size-tunable.[1] Therefore, nanocrystals have been used to improve the performance of organic light-emitting diodes,[2–3] to obtain single-photon sources operating at room temperature,[2b] and for the development of optically pumped laser devices.[3d,4] In addition to applications in light emitters, semiconductor nanocrystals have been used in hybrid solar cells.[3b,c,5] A hybrid solar cell, consisting of both conjugated polymers and inorganic semiconductor nanocrystals, combines the unique properties of inorganic semiconductors with the film-forming properties of conjugated polymers. There are two general concepts for making use of nanocrystals to improve polymer photovoltaic solar cells: The first is the bulk-heterojunction concept, in which charge-transfer junctions with high interfacial area are formed by blending semiconductor nanocrystals into conjugated polymers.[3b,c,5] Operation of such solar cells,

caused by photocurrent generation at the interface of nanocrystal/polymer composite materials, has been demonstrated in various blends containing CdSe,[3c] CuInS$_2$,[5] CdS,[6] and PbS[2b] nanocrystals. In the second concept, which is based on the Graetzel type of solar cells,[7] dyes are used for sensitizing a nanoporous TiO$_2$ film, which acts as an electrode in these devices. While in liquid-electrolyte-containing classical Graetzel cells, dyes like Ru-bipyridyl are used for light absorption and electron injection into the nanoporous TiO$_2$ conduction band, in solid-state dye-sensitized solar cells the liquid electrolyte is replaced by a layer of semiconductor like CuI[8,9] or CuSCN,[5b,7b] or by conjugated polymers.[10] In similar solid-state solar-cell structures nanocrystals instead of dyes have also been used for sensitizing the nanoporous electrodes.[11] The use of inorganic nanocrystals instead of organic dyes results in several advantages: the bandgap and, thereby, the absorption range are easily adjustable by the size of the crystals, as band-edge type of absorption behavior is the most favorable for effective light harvesting, and the surface properties of the particles can be modified in order to increase the photostability of the electrodes.[11b]

In this work, solar cells are fabricated both using HgTe nanocrystals deposited on nanoporous TiO$_2$ electrodes as well as by blending them into a hole-transporting polymer. Thus, we combine the solid-state nanocrystal-sensitized solar cell concept and the polymer/nanocrystal-blend solar cell concept, a combination which was never demonstrated before to the best of our knowledge. The combination of these two solar cell concepts results in: a) a higher photovoltaic response than that obtained from applying each concept individually using the same polymers and the same nanocrystals, and b) a shift of the photovoltaic response to longer wavelengths. The fabrication of such solar cells requires two types of nanocrystals: the first type must be miscible with the polymer and, thus, has to be soluble in organic solvents (referred hereafter as type OS). The second type, which is deposited on the TiO$_2$ electrode, should not be miscible with the polymer in order to avoid redissolving during

[*] Dr. S. Günes, Prof. N. S. Sariciftci, Dr. H. Neugebauer,
Linz Institute for Organic Solar Cells (LIOS), Physical Chemistry
Johannes Kepler University Linz, 4040 Linz (Austria)
E-mail: serap.guenes@jku.at; serdar.sariciftci@jku.at
J. Roither, M. Kovalenko, G. Pillwein, Prof. W. Heiss
Institute for Semiconductor and Solid State Physics
Johannes Kepler University Linz, 4040 Linz (Austria)

deposition of the polymer/nanocrystal blend on the nanocrystal-sensitized electrode. Thus, for the second type we make use of aqueous-soluble nanocrystals (hereafter referred as type AS). For both types we used colloidal HgTe nanocrystals stabilized, however, by different organic surface ligands. While bulk HgTe is a zero-gap semiconductor, the bandgap of chemically synthesized nanocrystals from this material lies in a broad tunable bandgap range depending on the particle size.[5c] Because of absorption related to this small bandgap, HgTe nanocrystals offer the advantage that a larger portion of the solar spectrum can be used for photovoltaics compared with the nanocrystals usually used in hybrid solar cells. One exception is a recent work, in which PbS nanocrystals were used to extend the spectral response of a hybrid solar cell up to a wavelength of 1600 nm.[2b] In comparison to the PbS-based bulk-heterojunction solar cells, however, our devices show a significantly higher photovoltaic response.

2. Results and Discussion

2.1. Solar Cell Structures and Morphology

The device presented here, which represents a combination of the concepts of a nanocrystal/polymer-blend solar cell and a solid-state nanocrystal-sensitized solar cell, and denoted as an "ASOS device", contains both types of nanocrystals, HgTe-AS and HgTe-OS. The ASOS device refers to aqueous soluble HgTe-AS nanocrystals coated onto nanoporous TiO₂ (NP-TiO₂) electrodes, which are further coated with organic-solvent-soluble HgTe-OS in a poly(3-hexylthiophene) (P3HT) matrix, as shown in Figure 1b. The electrodes, denoted as NP-TiO₂ electrodes throughout the paper, are a combination of a thin compact TiO₂ film prepared as described in the literature[12] and a nanoporous TiO₂ layer with a thickness of 800 nm. To study the photovoltaic response of the ASOS devices systematically, various reference cells were prepared for comparison. "Reference AS" is identical to the ASOS device but with only HgTe-AS nanocrystals on the NP-TiO₂ electrode and without HgTe-OS in P3HT. "Reference OS" was made with HgTe-OS nanocrystals in the polymer layer (nanocrystal/polymer blend) but without HgTe-AS nanocrystals on the NP-TiO₂ surface, and the "Reference-NO" solar cell was prepared without any nanocrystals.
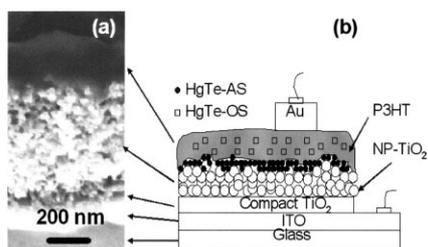
Figure 1. a) Cross-sectional scanning electron microscopy (SEM) image and b) sketch of the ASOS device, which combines the concepts of a solid-state nanocrystal-sensitized solar cell and a nanocrystal/polymer-blend solar cell. ITO: indium tin oxide.

The size distribution of the HgTe nanocrystals was found to be between 3 and 6 nm, as determined from section analysis of atomic force microscopy (AFM) measurements, performed on nanocrystal films on glass substrates. These values are in good agreement with the results obtained from transmission electron microscopy (TEM) of HgTe nanocrystals emitting at the same wavelengths as those used in this work.[1b]

For characterization of the device structures, we performed scanning electron microscopy (SEM) measurements on both device cross sections and on layer surfaces (plan views). By analyzing the SEM cross sections, the thicknesses of the individual layers are controlled and the penetration of the polymer/nanocrystals into the underlying porous layers was studied, as exemplified in Figure 1a for the ASOS device. As shown, drop-casting of the polymer results in a film thickness of approximately 300 nm. The polymer/TiO₂ interface is strongly corrugated whereby, near their interface, all the holes in the NP-TiO₂ layer are completely filled by the nanocrystal/polymer blend. The covering of the NP-TiO₂ surface with HgTe-AS is shown in more detail by the plan-view images presented in Figure 2. Figure 2a shows that the bare NP-TiO₂ electrode has two kinds of pores: pores with lateral dimensions on the order of 100 nm, and much smaller pores located between the TiO₂ grains that are smaller than the grain size of
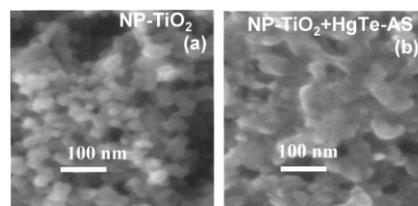
Figure 2. Plan-view SEM images of a) a bare NP-TiO₂ electrode and b) an NP-TiO₂ electrode treated with an aqueous solution of HgTe-AS nanocrystals.

50 nm. After immersion in the aqueous HgTe-AS solution for 12 h, at least the smaller pores at the interface are completely filled with nanocrystals (see Fig. 2b).

2.2. Photovoltaic Response

The photovoltaic properties of the solar cells were characterized by measuring current–voltage (I–V) curves in the dark and under simulated white-light illumination (AM1.5, 100 mW cm⁻²; AM: air mass) through the ITO side (ITO: indium tin oxide). Without illumination, all devices showed diode-like I–V curves, as shown in Figures 3a,c,e, and g, which are plotted on a semilogarithmic scale. A remarkable result we found is that incorporation of the HgTe nanocrystals improves the rectification of the diodes, since under reverse bias the dark currents of device ASOS and the cells Reference AS and Reference OS are much smaller than that of the reference without nanocrystals. Under illumination and reverse bias, the current
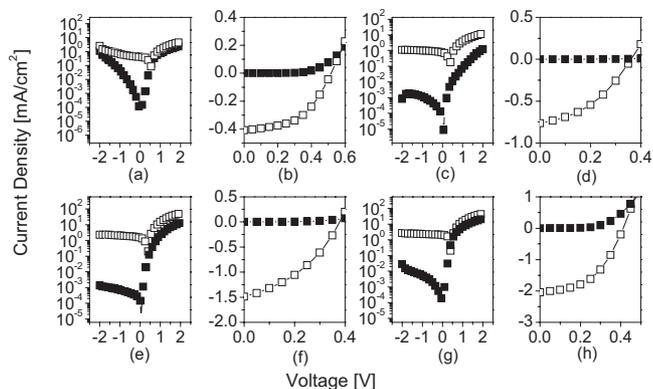
Figure 3. *I–V* characteristics of hybrid solar cells in the dark (filled-in symbols) and under simulated AM1.5 (100 mW cm⁻²) illumination (open symbols) on semilogarithmic and linear scales: a,b) Reference NO without any HgTe nanocrystals; c,d) Reference AS with nanocrystals at NP-TiO₂ surface; e,f) Reference OS with nanocrystals embedded in the polymer; and g,h) device ASOS in which the nanocrystal-sensitized and nanocrystal/polymer-blend concepts are combined.

increased by several orders of magnitude, proving the high photosensitivity of the solar cells. The characteristic parameters of the solar cells were deduced from the *I–V* curves plotted on linear scales, as shown in Figures 3b,d,f, and h. For device ASOS an open-circuit voltage (V_{oc}) of 400 mV, a short-circuit current density (I_{sc}) of around 2 mA cm⁻², and a fill factor of 0.5 were obtained. The power-conversion efficiency was calculated to be 0.4 % under simulated AM1.5 illumination. Device ASOS also gave a better photovoltaic performance than Reference AS and Reference OS, which contained, respectively, nanocrystals on the NP-TiO₂ surface or in the polymer only. For Reference AS, values of V_{oc} = 350 mV, I_{sc} = 0.8 mA cm⁻², and a fill factor of 0.4 were obtained, whereas for Reference OS V_{oc} = 400 mV, I_{sc} = 1.4 mA cm⁻², and a fill factor of 0.36 were obtained. The Reference NO cell, which did not contain any HgTe nanocrystals, exhibited values of V_{oc} = 500 mV and I_{sc} = 0.4 mA cm⁻² (fill factor of 0.5). These results show that the improvement in photovoltaic performance related to the incorporation of HgTe nanocrystals is mainly due to the increase of the short-circuit current.

2.3. Absorption Characteristics

By comparing the spectral response of the solar cells and the optical absorption spectra of the components of the devices, information on the charge-generation mechanism can be obtained. The glass substrates, the ITO contact layer, and the nanoporous TiO₂ were found to be sufficiently transparent in the whole operating spectral range of our devices, from 370 to 1500 nm. P3HT shows a broad absorption peak with a maximum at 553 nm and is almost transparent to wavelengths longer than 670 nm, as shown in Figures 4a and b. The HgTe nanocrystals show a weak absorption peak at long wavelengths close to 1400 nm, as measured for the HgTe-OS nanocrystals
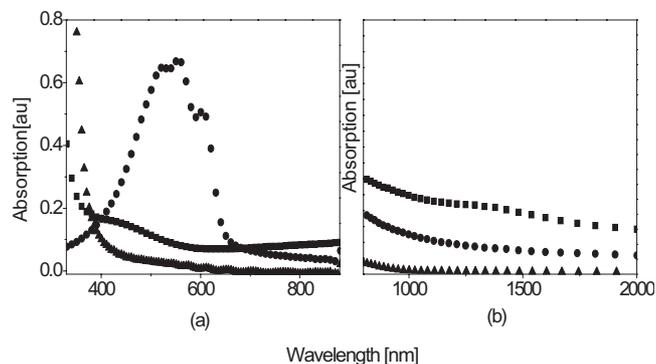

Figure 4. Absorption spectra of TiO₂ (▲), HgTe-OS(■), and P3HT(●). The different wavelength regions shown in (a) and (b) are measured using different experimental setups.

(Fig. 4b). This absorption corresponds to the fundamental optical transition across the bandgap of the nanocrystals with sizes in the range 3–6 nm. At shorter wavelengths absorption caused by transitions into excited nanocrystal states is observed.

2.4. Incident-Photon-to-Current Efficiency

The photoresponses of References NO, AS, and OS and the ASOS device are shown by the spectral dependence of the incident-photon-to-current efficiency (IPCE) curves in Figure 5. The percent IPCE is the percentage of electrons, measured under short-circuit current conditions, that are related to the number of incident photons,[13] and is used to ob-
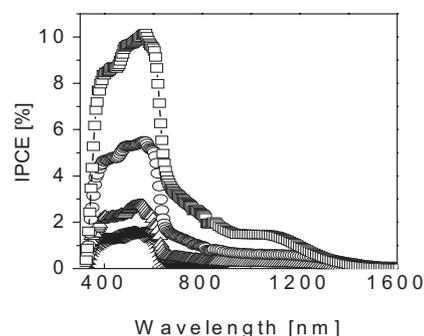

Figure 5. IPCE of device ASOS (□), and references OS (○), AS (△), and NO (×).

tain information on the number of photons of different energy that contribute to charge generation in the solar cell. The reference sample without nanocrystals (Reference NO) shows a photoresponse only at wavelengths shorter than 650 nm and with a maximum IPCE of 1.6 %. Incorporating nanocrystals into the P3HT (Reference OS) increases the photoresponse in the visible spectral range and sensitizes the spectral region at wavelengths longer than 650 nm. By add-

FULL PAPER

ing nanocrystals at the NP-TiO$_2$/P3HT interface (device ASOS) the photoresponse is further increased, resulting in a maximum IPCE of 10 % at wavelengths around 550 nm. For Reference AS, the maximum response is 2.5 %. The broad IPCE feature, which exists in the response of the solar cells at wavelengths shorter than 670 nm with a maximum around 550 nm, is related to both the P3HT absorption (see Fig. 4a) and the additional absorption offered by the HgTe nanocrystals that is caused by transitions into nanocrystal excited states that improve the IPCE. For the HgTe-containing devices, the photoresponse is extended to wavelengths in the IR up to 1500 nm. The response of the cells at these long wavelengths is attributed to the HgTe nanocrystals only, since the cell Reference NO, which contains no nanocrystals, does not show any response at wavelengths longer than 670 nm (see Fig. 5). The onset of the IPCE curve around 1500 nm corresponds to the bandgap of the HgTe nanocrystals. The results show that the HgTe nanocrystals are optically active both in the P3HT layer (type OS) as well as at the NP-TiO$_2$/P3HT interface (type AS).

For efficient charge transfer, the lowest unoccupied molecular orbital (LUMO) of the electron donor should be energetically located above the conduction band of TiO$_2$ as electron acceptor. It is difficult to determine the energy levels of HgTe nanoparticles. Tedious electrochemical methods led to incorrect results in our case. Therefore, the exact energetic mechanism for the improvement in charge generation obtained by adding nanocrystals is still under discussion. However, some additional effects should be taken into account for improving the efficiency: In the spectral range where P3HT absorbs, there is an additional absorption offered by HgTe nanocrystals that contributes to the charge-carrier generation. Also, the extension of the spectral range of the devices in the IR arises because of the absorption by HgTe, since the devices without nanocrystals do not show any response in the IR. In addition, HgTe-AS nanocrystals may help to reduce the interfacial charge-carrier recombination at the NP-TiO$_2$ interface, making the combination of both solar cell concepts more efficient than the individual concepts with a power-conversion efficiency of 0.4 % under simulated AM1.5 conditions.

3. Conclusion

We have demonstrated a novel concept for a nanocrystal-based hybrid solar cell, where HgTe nanocrystals are used to improve the photovoltaic performance of the cells as well as to extend the spectral region of operation up to 1500 nm. HgTe nanocrystals offer the possibility to push the wavelength-operation limit of hybrid solar cells to even longer wavelengths, which are not accessible by conventional dyes or most conjugated polymers, making such hybrid devices interesting not only for solar cells, but also for IR-sensitive hybrid photodetectors.

4. Experimental

4.1. Synthesis of HgTe-AS

Water-soluble HgTe nanocrystals were produced by precipitation reaction of Hg^{2+} (this is highly toxic) and Te^{2-} in the presence of thioglycerol as a surface-capping hydrophilic ligand, similarly to the procedure described in the literature [1b]. In a typical experiment, a 200 mL aqueous solution of 1.65 g of Hg(ClO$_4$)$_2$·3H$_2$O (Alfa) and 0.88 mL of thioglycerol (Aldrich) at pH 10 was loaded into a 250 mL three-necked flask and deaerated by bubbling with N$_2$ for 30 min. Subsequently, an appropriate amount of H$_2$Te gas was passed through the precursor solution. The final molar ratio of Hg^{2+}/Te^{2-}/RS$^-$ was set to 1:0.5:2.9.

4.2. Preparation of HgTe-OS

The HgTe-OS nanocrystals were obtained by a ligand-exchange procedure [1b] that made use of the HgTe-AS nanocrystals. For this, 10 mL of the as-prepared solution of thioglycerol-capped HgTe-AS nanocrystals was placed into a vessel, to which a mixture of 5 mL of dodecanethiol and 5 mL of acetone was added. The vessel was tightly closed and heated to 70 °C for 5 min under vigorous stirring. Afterwards, 2–3 mL of methanol was added to facilitate the separation of the emulsion into an aqueous phase on the bottom with an organic phase containing nanocrystals on top. The organic phase was extracted and washed several times with methanol, giving the precipitate of dodecanethiol-capped HgTe nanocrystals. HgTe-OS nanocrystals were additionally purified by repetitive dissolving in hexane followed by precipitation with methanol and centrifugation of the resulting flocculate. Prior to the last precipitation of HgTe-OS, the nanocrystals were filtered through a 0.2 μm poly(tetrafluoroethylene) (PTFE) filter. Finally, HgTe-OS nanocrystals were dried under vacuum and dissolved in chloroform.

4.3. Cell Preparation and Experimental Methods

For sample preparation, first a compact TiO$_2$ layer was prepared onto ITO-coated (ITO: indium tin oxide) glass substrates by spin-casting a sol–gel solution of titanium isopropoxide in ethanol as described in the literature [12]. The compact TiO$_2$ layer was sintered at 450 °C for 30 min in air. On top, a nanoporous TiO$_2$ film was prepared by doctor-blading a diluted TiO$_2$ paste (Solaronix Co. Switzerland) and sintering for a second time at 450 °C for 30 min. This resulted in a film with a thickness of about 800 nm on top of a ca. 100 nm compact TiO$_2$ layer. The electrodes consisting of compact TiO$_2$ and a nanoporous TiO$_2$ layer are denoted as NP-TiO$_2$ electrodes. The nanocrystal sensitization was done by treating NP-TiO$_2$ electrodes with HgTe-AS nanocrystals for 12 h. Although the Hg^{2+} ion is highly toxic, we rinsed the HgTe-AS-covered electrodes with water. Therefore, our devices were not contaminated with Hg^{2+} ions. As a hole-conducting conjugated polymer we used poly(3-hexylthiophene) (P3HT) which was dissolved in chlorobenzene with a 1 % weight concentration. The nanocrystal/polymer blend was prepared by mixing HgTe-OS and P3HT in a weight ratio of 2.2:1. This is the experimentally optimized ratio. The ratio of nanocrystals in the blend was 35 %. The active layers of all cells were deposited by drop-casting. Device ASOS was prepared by treating NP-TiO$_2$ electrodes with HgTe-AS nanocrystals for 12 h and drop-casting the HgTe-OS/P3HT blend on the treated electrodes. Reference OS consisted of a HgTe-OS/P3HT blend on top of a bare NP-TiO$_2$ electrode. Reference AS was prepared by treating the NP-TiO$_2$ electrodes with HgTe-AS nanocrystals and drop-casting P3HT. Reference NO was prepared without any HgTe nanocrystals and consisted of bare NP-TiO$_2$ electrodes and P3HT, and, finally, 160 nm Au was thermally evaporated. In

all device configurations we chose gold as the top-electrode material because its work function is close to the highest molecular orbital (HOMO) of the hole conductor, P3HT. Thus, hole injection from the polymeric organic material into the metal electrode is energetically possible.

4.4. Electron Microscopy and Photovoltaic Characterization

The scanning electron microscopy (SEM) analysis was done using a LEO Supra 35 scanning electron microscope.

All current–voltage (*I–V*) characteristics of the devices were measured (using a Keithley SMU 236 unit) under inert atmosphere conditions (argon) in a dry glove box immediately after production. A Steuernagel solar simulator, under air mass (AM) 1.5 conditions, was used as the excitation source with an output power of 100 mW cm^{-2} white-light illumination. For the electrical characterization, the cells were illuminated through the ITO side.

4.5. Photoresponse Experiments

For measuring IPCE response between 300 and 900 nm the samples were illuminated under argon atmosphere inside a glovebox with light from a Xenon lamp passing a monochromator (full width at half maximum ca. 4 nm, illumination intensity ranging between ~50 and ~200 µW cm^{-2}) and chopped at a frequency of 273 Hz. Using an EG&G Instruments 7260 lock-in amplifier, the photocurrent of the solar cell was related to the photon flux, which was determined using a calibrated Si detector. The IR response was characterized by using a 15 cm grating spectrometer and an InSb detector. To eliminate quantification inconsistencies between the UV-vis and the IR measurement setup, the *y*-axis of the IPCE curve was scaled to the same value as that obtained with the silicon reference diode at 900 nm.

[1] a) D. V. Talapin, A. L. Rogach, A. Kornowski, M. Haase, H. Weller, *Nano Lett.* **2001**, *1*, 207. b) N. Gaponik, D. V. Talapin, A. L. Rogach, A. Eychmüller, H. Weller, *Nano Lett.* **2002**, *2*, 80.

[2] a) V. L. Colvin, M. C. Schlamp, A. P. Alivisatos, *Nature* **1994**, *370*, 354. b) P. Michler, A. Imamoglu, M. D. Mason, P. J. Carson, G. F. Strouse, S. K. Buratto, *Nature* **2000**, *406*, 968. c) S. McDonald, G. Konstantatos, S. Zhang, P. W. Cyr, E. J. D. Klem, L. Levina, H. Sargent, *Nat. Mater.* **2005**, *4*, 138.

[3] a) N. Tessler, V. Medvedev, M. Kazes, S. H. Kan, U. Banin, *Science* **2002**, *295*, 1506. b) A. P. Alivisatos, *Science* **1996**, *271*, 933. c) W. Huynh, J. Dittmer, A. P. Alivisatos, *Science* **2002**, *295*, 2425. d) V. I. Klimov, A. A. Mikhailovsky, A. V. Malko, J. A. Hollingsworth, C. A. Leatherdale, H.-J. Eisler, M. G. Bawendi, *Science* **2000**, *290*, 314.

[4] a) A. A. Mikhailovsky, A. V. Malko, J. A. Hollingsworth, M. G. Bawendi, V. I. Klimov, *Appl. Phys. Lett.* **2002**, *80*, 2380. b) H.-J. Eisler, V. C. Sundar, M. G. Bawendi, M. Walsh, H. I. Smith, V. I. Klimov, *Appl. Phys. Lett.* **2002**, *80*, 4614. c) A. V. Malko, A. A. Mikhailovsky, M. A. Petruska, J. A. Hollingsworth, H. Htoon, M. G. Bawendi, V. I. Klimov, *Appl. Phys. Lett.* **2002**, *81*, 1303.

[5] a) E. Arici, N. S. Sariciftci, D. Meissner, *Adv. Funct. Mater.* **2003**, *13*, 165. b) B. O'Regan, D. T. Schwartz, S. M. Zakeeruddin, M. Graetzel, *Adv. Mater.* **2000**, *12*, 1263. c) A. Rogach, S. Kerschaw, M. Burt, M. Harrison, A. Kornowski, A. Eychmüller, H. Weller, *Adv. Mater.* **1999**, *11*, 552.

[6] N. C. Greenham, X. Peng, A. P. Alivisatos, *Phys. Rev. B* **1996**, *54*, 17 628.

[7] a) M. K. Nazeeruddin, A. Kay, I. Rodicio, R. Humphry-Baker, E. Müller, R. Liska, N. Vlachopoulos, M. Graetzel, *J. Am. Chem. Soc.* **1993**, *115*, 6382. b) B. O'Regan, D. T. Schwartz, *Chem. Mater.* **1997**, *9*, 439.

[8] K. Tennakone, G. R. R. A. Kumara, I. R. M. Kottegada, K. G. U. Wijayantha, P. M. Sirimanne, *Semicond. Sci. Tech.* **1995**, *10*, 1689.

[9] K. Tennakone, G. R. R. A. Kumara, I. R. M. Kottegada, M. Wijayantha, V. P. S. Perera, *J. Phys. D* **1999**, *32*, 374.

[10] D. Gebeyehu, C. J. Brabec, N. S. Sariciftci, D. Vangenuegden, R. Kiebooms, D. Vanderzende, F. Kienberger, H. Schindler, *Synth. Met.* **2002**, *125*, 279.

[11] a) D. Liu, V. P. Kamat, *J. Phys. Chem.* **1994**, *98*, 3183. b) R. Vogel, P. Hoyer, H. Weller, *J. Phys. Chem.* **1994**, *98*, 3183.

[12] L. Kavan, M. Grätzel, *Electrochim. Acta* **1995**, *40*, 643.

[13] J. Rostalski, D. Meissner, *Sol. Energy Mater. Sol. Cells* **2000**, *61*, 87.